ACS OMEGA

http://pubs.acs.org/journal/acsodf

Article

New Insight into Temperature Effects on Low-Rank Coal Flotation Using Diesel as a Collector

Xicheng Bao,* Junling Liu, Shasha Wang, Dongqin Chen, Wenjin Xu, Deke Zhang, Jihui Li, Yaowen Xing, and Mengdi Xu*

Cite This: *ACS Omega* 2023, 8, 15479−15487

Read Online

ACCESS | Metrics & More | Article Recommendations

ABSTRACT: Efficient flotation of low-rank coal is of great significance for the development of green and low-carbon cycles. Temperature is a crucial parameter of flotation, but the mechanism of its effect on flotation lacks understanding. In this paper, the mechanism was studied by kinetic flotation, scanning electron microscopy (SEM), Fourier transform infrared spectroscopy, low-temperature liquid-nitrogen adsorption (LP-N_2A), X-ray photoelectron spectroscopy (XPS), and molecular dynamics simulation. The flotation combustible recovery gradually decreases as temperature rises. Compared with 60 °C, the combustible recovery at 5 °C increases by 18.13%. The desorption energy for oil droplets decreases as the temperature rises. As a result, the oil droplets are easier to desorb at high temperatures. The SEM and LP-N_2A results demonstrate that the pores and fractures of the coal sample are well developed. Also, the oil−water interfacial tension and viscosity of oil droplets decrease as the temperature rises, while the diffusion ability increases. These increase the volume of oil droplets that penetrate into the pores, resulting in poor spreadability of oil droplets on the coal surface. The average volume of bubbles gradually increases as temperature rises, which renders the flotation foam unstable and worsens the flotation. Therefore, the flotation performance is better at low temperatures.

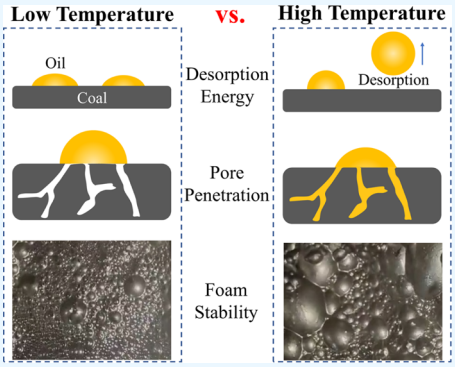

1. INTRODUCTION

As a low-grade resource, the processing of low-rank coal (LRC) has been paid more and more attention.[1−3] Efficient and full utilization of LRC is of great significance to understand green and low-carbon cycle development.[4−6] Flotation plays an important role in the recovery of fine-grained LRC.[7−10] However, the flotation efficiency still needs to be improved, and there is an urgent need to find more factors restricting flotation and solve it.[11−16]

Some scholars focus on the new high-efficiency collectors, mainly focusing on the research of polar collectors and compound collectors. The results show that the polar collector can cover the oxygen-containing sites on the surface of LRC and improve the surface hydrophobicity of LRC, so the clean coal yield of flotation is improved.[17−26] In addition, the synergistic effect of polar and nonpolar components in the compound collector further strengthens the flotation.

Some scholars strengthen flotation by improving the fluid environment.[27−32] Wang et al.[30] proposed a new technique for improving coal flotation by employing impact flow conditioning pulp, and the impact velocity of the conditioning pulp was tuned, resulting in improved flotation and cleaner coal output. Han et al.[31] proposed a jet-stirring coupling flotation device, and it was shown to have a considerable effect on boosting gas holdup and decreasing bubble size. Li et al.[32] designed a new type of flow mixer without an agitator and carried out pretreatment experiments on pulverized coal with different quenching and tempering times. The results show that fluid strengthening has a positive effect on the improvement of surface hydrophobicity.

However, few scholars have mentioned the effect of temperature on coal flotation. In the past 5 years, there is only one paper mentioned, but there are only flotation kinetics tests and no mechanism study.[33] Therefore, it can be inferred that the mechanism of the effect of temperature on flotation lacks understanding. In this paper, the effect mechanism of temperature on the flotation of LRC was studied by kinetic flotation, scanning electron microscopy (SEM), Fourier transform infrared spectroscopy (FTIR), low-temperature liquid-nitrogen adsorption (LP-N_2A), X-ray photoelectron spectroscopy (XPS), and molecular dynamics (MD) simulation, which provides theoretical guidance for industrial production.

Received: February 6, 2023
Accepted: April 11, 2023
Published: April 23, 2023

2. MATERIALS AND METHODS

2.1. Materials. LRC samples were taken from Ordos Zhuanlongwan Coal Co., Ltd., of China Co., Ltd., and the proximate analysis of LRC samples is shown in Table 1. It can be seen from Table 1 that the moisture, ash, volatile, and fixed carbon contents of the coal sample are 6.05, 19.18, 26.47, and 48.30%, respectively. The moisture content of LRC samples is as high as 6.05%, indicating that the pores are developed. The fixed carbon content of this coal is low, and the volatile content reaches 26.47%, so it is a typical LRC.

Table 1. Proximate Analyses of the LRC Samples (Ad: Air Dry Basis)

proximate analysis (wt %)			
Mad	Aad	Vad	FCad
6.05	19.18	26.47	48.30

In the experiment, diesel and 2-octanol ($C_8H_{18}O$), purchased from Aladdin Co., Ltd., were used as flotation agents.

2.2. Kinetic Flotation Experiments. The flotation experiments were carried out in a 1.0 L XFD laboratory flotation cell. The amount of collector diesel oil was 4 kg/t. The amount of foaming agent secondary octanol was 1 kg/t. The pulp mass concentration was 80 g/L. The aeration volume was 0.1 m^3/h. The rotation speed of the flotation cell was 1800 r/min, and the kinetic flotation experiments were conducted at the pulp temperatures of 5, 10, 20, 40, and 60 °C. The flotation experiments were carried out when the room temperature was less than 5 °C in winter, and the flotation temperature was controlled to the required temperature before the start of each flotation experiment. A temperature-controlled silicone rubber heating plate affixed around the flotation cell was utilized to maintain the flotation temperature stable within a range of ±1 °C of the required temperature, which was purchased from Shanghai Songdao Heating Sensor Co., Ltd. The kinetic flotation test process was as follows: first, the coal sample was added for slurry mixing for 120 s, then the collector and the foaming agent were added in turn, they were reacted for 120 and 30 s, respectively, and the foam was scraped five times, with scraping times of 30, 30, 60, 60, and 120 s. Finally, each product was collected for filtering, drying, sample preparation, and ash burning, and the products obtained were J1, J2, J3, J4, and J5, respectively. After starting to produce concentrate foam, industrial cameras were used to capture foam images.

2.3. SEM Tests. SEM was used to scan the sample surface by electron beam, secondary electronic signals generated by excitation were collected, and the surface morphology information of the sample was obtained. The pore, crack, and other morphology of the coal surface can be observed visually by SEM. A proper amount of the coal sample was taken, ultrasonically dispersed in anhydrous ethanol for 1 min, shaken evenly, absorbed with a rubber tip dropper, smeared on a clean glass sheet, and dried at low temperature for testing.

2.4. FTIR Tests. FTIR spectroscopy can be used to study the molecular structure and chemical bond type, measure the molecular bond length, speculate the molecular stereo-configuration, determine the organic functional group composition in the sample, and so forth, and it lays the foundation for the final determination of the sample chemical structure. 0.074 mm particles were sieved; infrared spectrum analysis of the coal sample was performed, and the chemical functional group composition of the coal sample was detected. According to the intensity and position of the characteristic absorption peak, the type of functional group contained in the coal sample can be judged by the infrared spectrum test of the coal sample.

2.5. LP-N_2A Measurements. The experiment was conducted using a standard degassing station from Micromeritics and a 4-station fully automated surface area analyzer, model APSP 2460, under vacuum conditions at 120 °C. The sample was pretreated for 12 h and subjected to nitrogen adsorption/desorption tests at 77 K under liquid nitrogen using the aforementioned analyzer. The resulting isotherms were analyzed using the Brunauer−Emmett−Teller (BET) method to determine the total surface area of the material. This experimental procedure has not been reported in previous literature.

2.6. XPS Tests. The surface of coal was analyzed and tested by XPS to understand its surface functional group composition. The coal sample was added to mix the slurry at 5, 10, 20, 40, and 60 °C for 120 s, and then diesel oil was added to react for 120 s to obtain five products. The obtained product was filtered and dried, and the coal sample was screened below 0.074 mm for XPS tests. As a comparison, untreated raw coal was tested.

2.7. MD Simulation. The LRC model's repeating unit of the surface structure, as seen in Figure 1, was created by Materials Studio 8.0 developed by Accelrys, Inc. The repeating unit was then expanded into an entire LRC surface model by using the supercell feature of Materials Studio. The LRC surface model and the directly established three-layer graphite structure were joined to form the full LRC model, which has been used in many papers to make it easier to understand how LRC and collectors interact.[34−39]

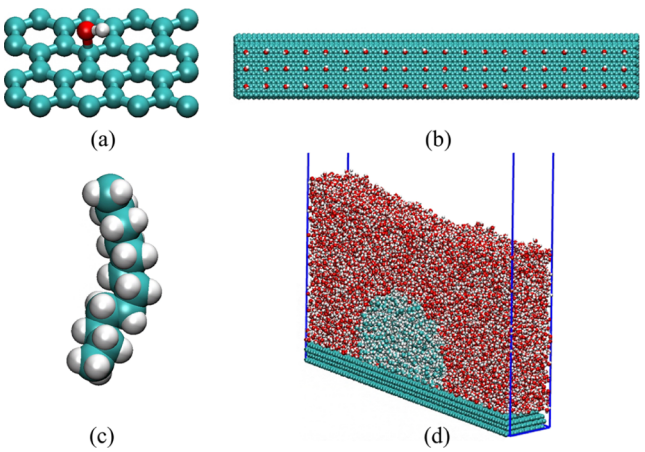

Figure 1. (a) LRC surface repeating unit, (b) LRC model, (c) dodecane molecule, and (d) initial configuration of the oil droplet spreading simulation system.

The OPC3 water model was used for simulation, which is better than SPCE in many aspects.[40] Diesel was replaced with dodecane.[8] Other molecules were described using the general AMBER force field[41] (GAFF), and MD simulations were all completed by the GROMACS 2019.6 software package.[42]

The mean restrained electrostatic potential charges in the liquid and gas phases of the LRC surface repeating unit and dodecane were computed by ORCA,[43] which is called

https://doi.org/10.1021/acsomega.3c00774
ACS Omega 2023, 8, 15479−15487

RESP2$_{0.5}$,[44] calculated by Multiwfn (version 3.7).[45] LRC model atoms except the hydroxyl functional group atoms are uncharged.[46] The topology files for GROMACS were prepared by Sobtop.[47]

A semicylindrical oil droplet with a diameter of 8 nm was placed on the LRC model, surrounded by enough water molecules, as shown in the figure. The curvature in the *Y* direction can be considered as 0, which avoids the line tension and makes the contact angle simulation more consistent with the macroscopic contact angle. There was enough vacuum layer above the system to avoid periodic influence. The final size of the box was 20.15 × 3.15 × 40 nm^3.

The energy of initial configurations was reduced by employing the steepest descent approach.[48] In the *NVT* ensemble, an MD simulation with a time step of 2 fs was run at 298 K. With a relaxation time constant of 0.1 ps, the v-rescale thermostat[49] was utilized to regulate the temperature. The H-bond lengths were constrained by the LINCS approach.[50] The *X*, *Y*, and *Z* directions used periodic boundary conditions. All of the hydroxyl groups in the LRC model were frozen. van der Waals interactions were calculated using the cutoff technique with a cutoff distance of 1.0 nm, whereas electrostatic interactions were calculated using the particle mesh Ewald[51] (PME) method. VMD 1.9.3 was used to show the simulation results.[52]

3. RESULTS

3.1. Characterization of Coal Properties. *3.1.1. SEM Results.* Figure 2 shows the SEM image of the coal sample. It

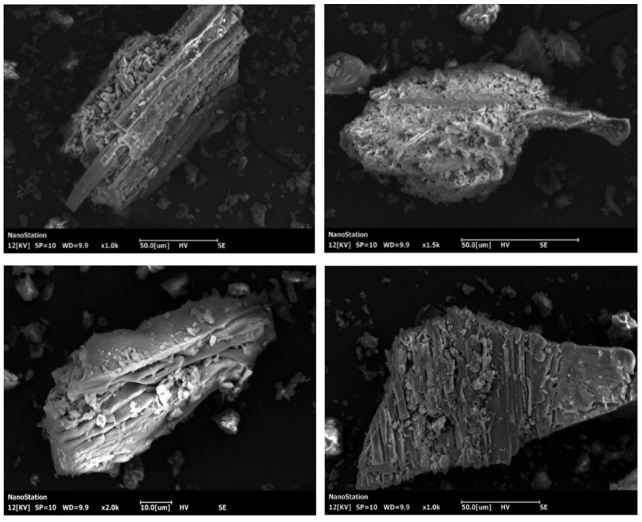

Figure 2. SEM image of the coal sample.

can be seen from the image that the surface of the coal sample is rough, and there are many cracks and pores on the surface of the coal sample. Developed fractures and pores will increase to a certain extent, which will increase the specific surface area of coal samples, thus increasing the consumption of the collector. At the same time, pores and cracks will affect the spread of the collector and even cause the collector to lose its effect.

3.1.2. FTIR Spectroscopy Results. The LRC has an obvious absorption peak near 3619 cm^{-1}, which can be attributed to the stretching vibration of the free hydroxyl (−OH) group (see Figure 3). The peak of LRC near 3191 cm^{-1} is attributed to the hydrogen bond formed by ring closely associated hydroxyl

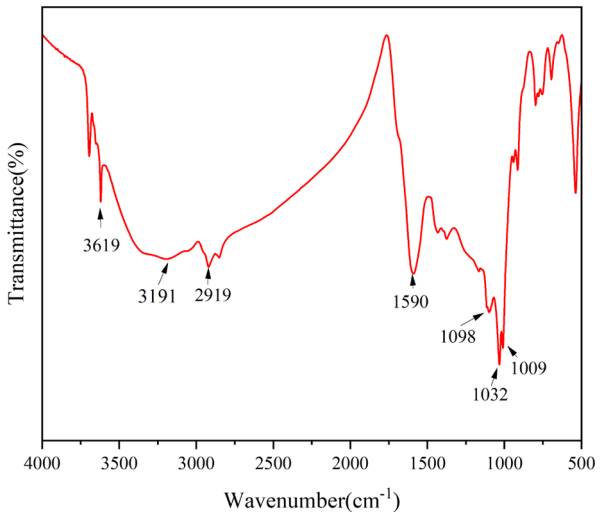

Figure 3. FTIR spectrum of the coal sample.

groups. The characteristic peak of LRC near 2919 cm^{-1} is that of the methyl (−CH$_3$) group stretching vibration peak. The peak of LRC at 1590 cm^{-1} is attributed to C═C stretching vibration in aromatic hydrocarbons. The peak of LRC at 1032 cm^{-1} is attributed to the Si−O stretching vibration. These components are prone to forming hydrogen bonds with water in the solution and have low hydrophobicity, making it difficult for nonpolar hydrocarbon oils to accumulate on the surface of these molecules, resulting in poor flotation performance.[53−56]

3.1.3. LP-N$_2$A Results. N$_2$ adsorption/desorption isotherms and the Barret−Joyner−Halenda (BJH) pore volume curve are shown in Figure 4. At the same time, the measurement results indicate that the BJH adsorption cumulative volume of pores between 1.7 and 300.0 nm diameter for the LRC sample under investigation was 0.019935 cm^3/g, and its BET specific surface area was 7.0346 m^2/g. Compared to LRC reported in the literature, the coal sample exhibited a higher specific surface area.[57,58] In general, LRCs possess certain pore volumes due to their low degree of metamorphism.[59] Based on the recommended IUPAC pore classification method, the pores in coal can be divided into micropores (<2 nm), mesopores (2−50 nm), and macropores (>50 nm). As shown in Figure 4b, this LRC sample contains an amount of macropores. In the flotation process, pores have a certain reagent consumption capacity.

3.2. Kinetic Flotation Results. The kinetic flotation data are fitted by the first-order kinetic flotation equation, and the fitting results are shown in Figure 5. It has a good fitting effect at five temperatures, and R^2 is greater than 0.99.

In the first 1 min, the flotation rate at 5 °C is close to that at 10 °C, and then the flotation rate slows down with the increase in temperature. The final combustible recovery rate gradually decreases with the increase of temperature. This shows that the increase of temperature is not conducive to the flotation of LRC; on the contrary, higher recovery of combustible recovery can be obtained at a lower temperature. Compared with 60 °C, the combustible recovery in flotation at 5 °C increases by 18.13%.

The cumulative ash content curve of clean coal is shown in Figure 6, and the final ash content of clean coal increases with temperature. In other words, the higher the flotation combustible recovery is, the lower the content of clean coal

https://doi.org/10.1021/acsomega.3c00774
ACS Omega 2023, 8, 15479−15487

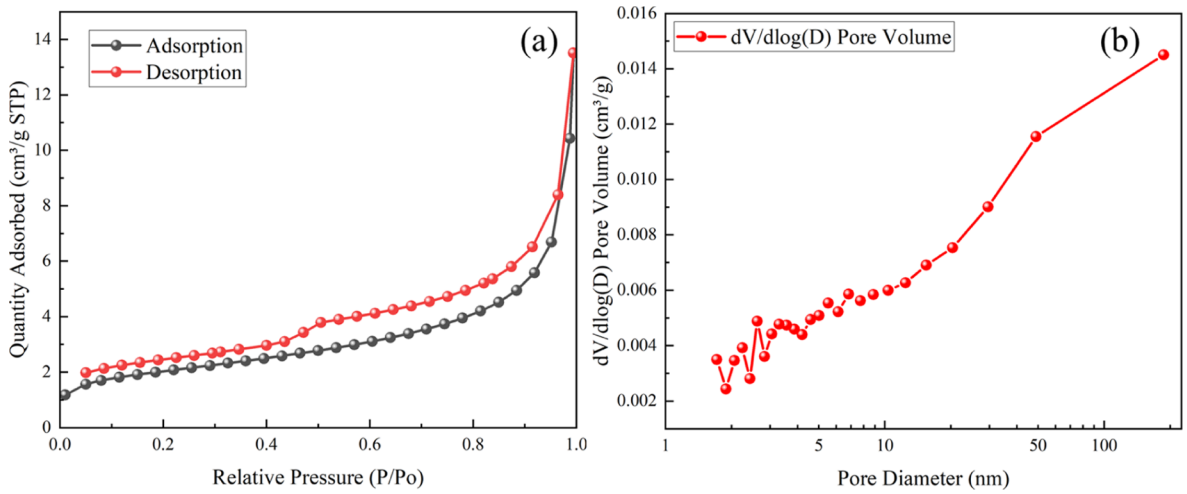

Figure 4. (a) N_2 adsorption/desorption isotherms and (b) distribution curves of the BJH adsorption pore volume.

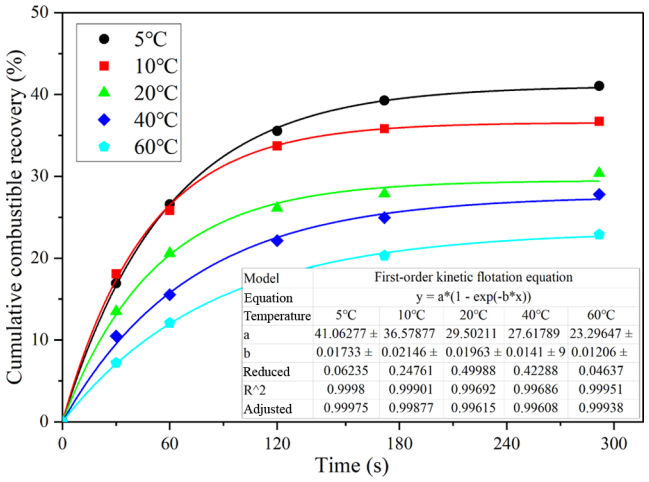

Model	First-order kinetic flotation equation				
Equation	y = a*(1 - exp(-b*x))				
Temperature	5°C	10°C	20°C	40°C	60°C
a	41.06277 ±	36.57877	29.50211	27.61789	23.29647 ±
b	0.01733 ±	0.02146 ±	0.01963 ±	0.0141 ± 9	0.01206 ±
Reduced	0.06235	0.24761	0.49988	0.42288	0.04637
R^2	0.9998	0.99901	0.99692	0.99686	0.99951
Adjusted	0.99975	0.99877	0.99615	0.99608	0.99938

Figure 5. Kinetic flotation results and the first-order kinetic flotation equation fitting results.

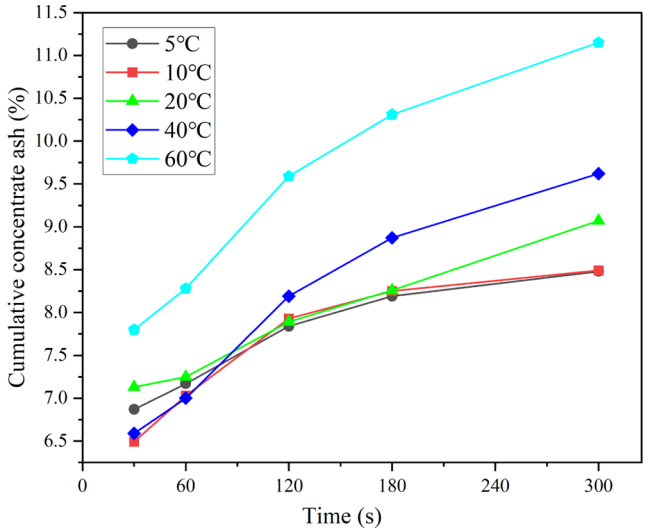

Figure 6. Cumulative ash content curve of clean coal.

ash is, which is a characteristic of LRC flotation. However, this characteristic is not obvious in the initial stage of flotation.

3.3. Flotation Foam Morphology. During the flotation process, the bubble image is recorded at the beginning of bubble generation, as shown in Figure 7. It can be clearly observed that the number of large bubbles increases as the temperature rises. At 5 °C, the bubbles are small, uniform, and dense. However, at 60 °C, the bubbles become uneven, and large bubbles dominate. This indicates that the increase of temperature leads to an increase in bubble volume, which will further cause bubbles to burst easily; that is, bubbles become unstable and worsen flotation.

3.4. XPS Results. The semiquantitative examination of the wide sweep element content reveals that the oxygen content is 33.41%, indicating that the coal sample has a high surface oxygen content (see Figure 8). The binding energies of the groups C−C/C−H, C−O, C═O, and O−C═O are 284.60, 285.60, 286.60, and 289.10 eV, respectively.[60,61] The ratios of C−C/C−H, C−O, C═O, and O−C═O are 45.92, 27.67, 20.61, and 5.80%, respectively. C−O is the main oxygen-containing group on the LRC surface. These oxygen-containing sites have strong polarity and can form hydrogen bonds with water, resulting in poor hydrophobicity.[62,63]

In order to conform to the flotation environment, XPS tests were carried out on coal samples after diesel pulping. Cai et al.'s study[64] shows that in the pulp environment (the oxygen content in the pulp is much lower than that in the air), the coal will hardly be oxidized in a short time. Therefore, it can be considered that the oxygen content of raw coal does not change with temperature during 120 s of pulping time.[64] At different temperatures, the oxygen content on the surface of coal after the action of diesel oil is shown in Figure 9. The surface oxygen contents of coals treated with diesel all are lower than that of raw coal. With the increase of temperature, the oxygen content on the coal surface increases gradually. This demonstrates that diesel has a certain covering effect on the oxygen sites on the surface of LRC, and this covering effect gradually weakens with the increase of temperature.

3.5. MD Simulation Results. *3.5.1. Contact Angle.* MD simulation was carried out at three temperatures of 5, 20, and 60 °C. After 10 ns, the simulation at three temperatures reached equilibrium. The ImageJ contact angle measurement tool was used to measure the contact angle. It can be seen from the results that the contact angle increases gradually as the temperature rises from 62.95 to 75.60° (see Figure 10). It can

https://doi.org/10.1021/acsomega.3c00774
ACS Omega 2023, 8, 15479−15487

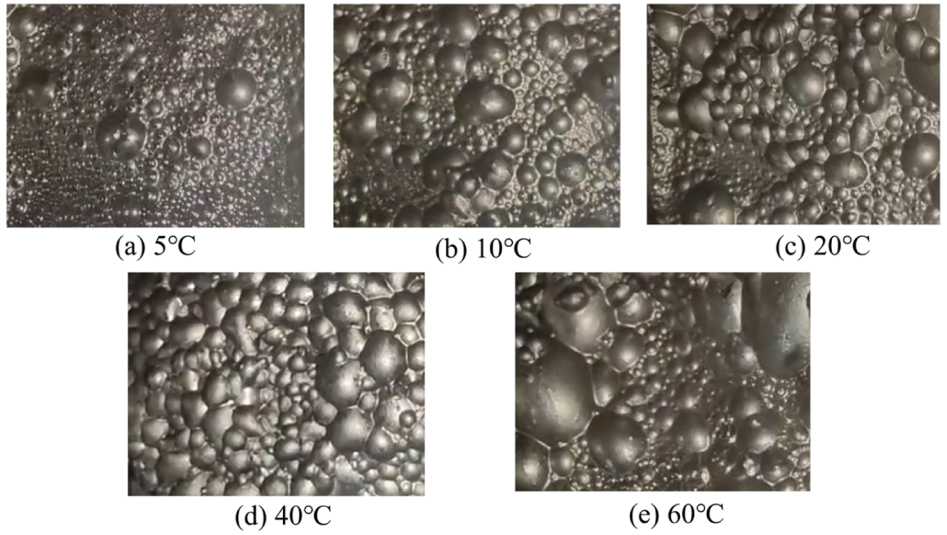

Figure 7. Bubble image at the beginning of bubble generation at different temperatures: (a) 5, (b) 10, (c) 20, (d) 40, and (e) 60 °C.

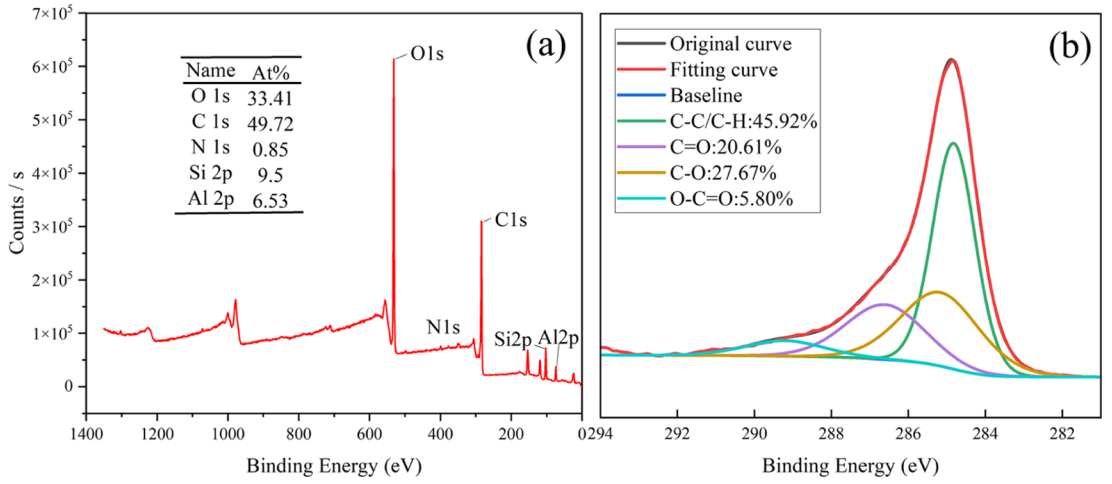

Figure 8. (a) XPS wide sweep spectra and (b) C 1s peak of the LRC sample.

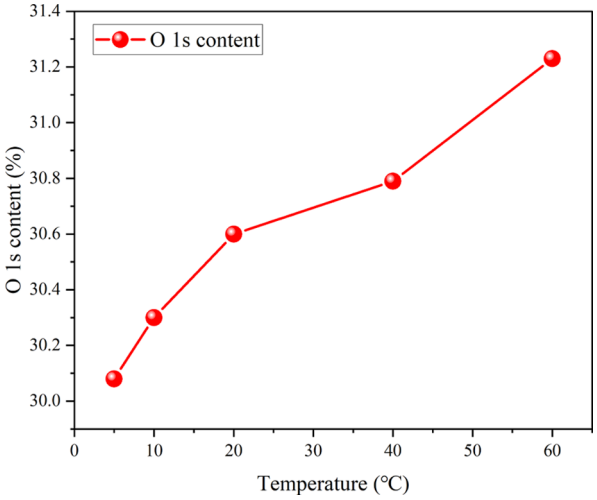

Figure 9. Effect of temperature on the oxygen content of the LRC surface after the action of diesel oil.

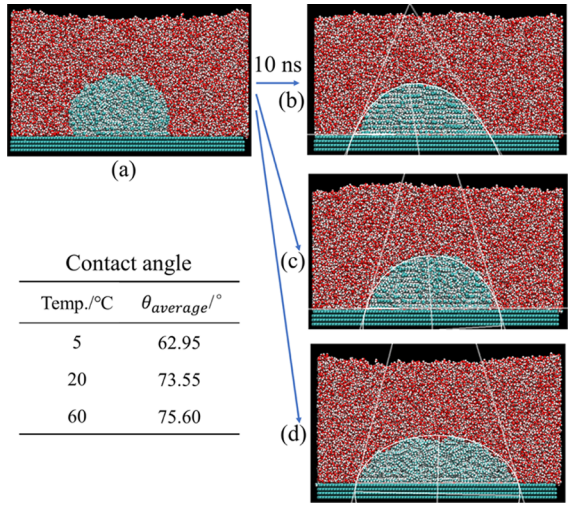

Figure 10. (a) Initial configuration and contact angle results of MD simulations at (b) 5, (c) 20, and (d) 60 °C (the white lines in the picture are traces of the contact angle calculated by ImageJ).

also be observed that at 60 °C, the oil droplets become more loosely expanded. Nevertheless, under the joint action of oil−water-LRC in the three-phase contact line, the contact angle at

https://doi.org/10.1021/acsomega.3c00774
ACS Omega 2023, 8, 15479−15487

the highest temperature is still the largest. The same conclusion has been reached in Zhang's[65] and Gayle's[66] studies.

3.5.2. Mean Square Displacement. The diffusion coefficient D is a measurement of the behavior of molecules in diffusion, and it is inversely proportional to how stable the adsorption of collector molecules on the coal surface is. The mean square displacement (MSD) is a function of time and quantifies the average of the squared particle displacements after t time. The diffusion coefficient D is 1/6 of the slope of the MSD curve.

5−10 ns of simulated trajectories were selected for MSD analysis. The MSD curves at three temperatures are shown in Figure 11 11, and the diffusion coefficient D was calculated at the same time. It can be clearly found from the calculation results that D gradually increases as temperature rises. This shows that at higher temperatures, the oil droplets have stronger diffusion ability but worse adsorption stability.

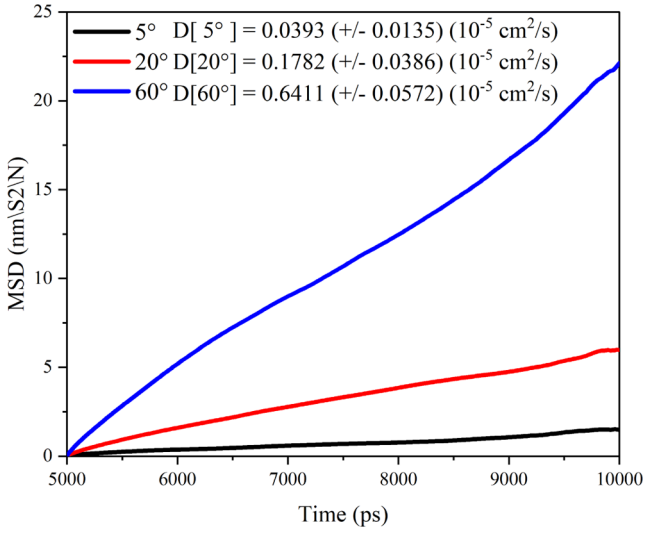

Figure 11. MSD and diffusion coefficient D results.

4. DISCUSSION

According to the test results, it can be determined that the direct reason for the poor flotation effect caused by the rise of temperature is that the function of the collector becomes invalid gradually.

Zhang et al.[65] studied the interactions of oil droplets with water-wetted shale kerogen and proposed linear relationships between temperature, free energy, and contact angle. This is very similar to the interactions between diesel and coal. Therefore, with reference to their study, we have deduced the desorption energy relationship between diesel and coal.

The desorption energy (F) per surface area (a) is equal to the interface tension (γ).[67]

$$dF = \gamma_{i-j} \cdot da_{i-j} \tag{1}$$

In the equation below, "c" denotes the coal surface; "o", diesel oil; "w", water; and "v", vacuum. Also, "u" and "′"stand for the unabsorbed oil droplet system and the adsorbed oil droplet system, respectively.

Equation 1 can be expanded as

$$dF = \gamma_{c-v} \cdot da_{c-v} + \gamma_{w-v} \cdot da_{w-v} + \gamma_{o-w} \cdot da_{o-w} + \gamma_{c-w} \cdot da_{c-w} + \gamma_{o-c} \cdot da_{o-c} \tag{2}$$

$$da_{w-v} = da_{c-v} = 0 \tag{3}$$

Free energy of desorption

$$\Delta F = F^{u} - F' = (\gamma_{o-w} \cdot a^{u}_{o-w} + \gamma_{c-w} \cdot a^{u}_{c-w}) - (\gamma_{o-w} \cdot a'_{o-w} + \gamma_{c-w} \cdot a'_{c-w} + \gamma_{o-c} \cdot a'_{o-c}) \tag{4}$$

$$a^{u}_{c-w} = a'_{c-w} + a'_{o-c} \tag{5}$$

So

$$\Delta F = \gamma_{o-w} \cdot (a^{u}_{o-w} - a'_{o-w}) + (\gamma_{c-w} - \gamma_{o-c}) \cdot a'_{o-c} \tag{6}$$

Young's equation describes the diesel oil contact angle (θ).[68]

$$\gamma_{c-w} - \gamma_{o-c} = \gamma_{o-w} \cdot \cos\theta \tag{7}$$

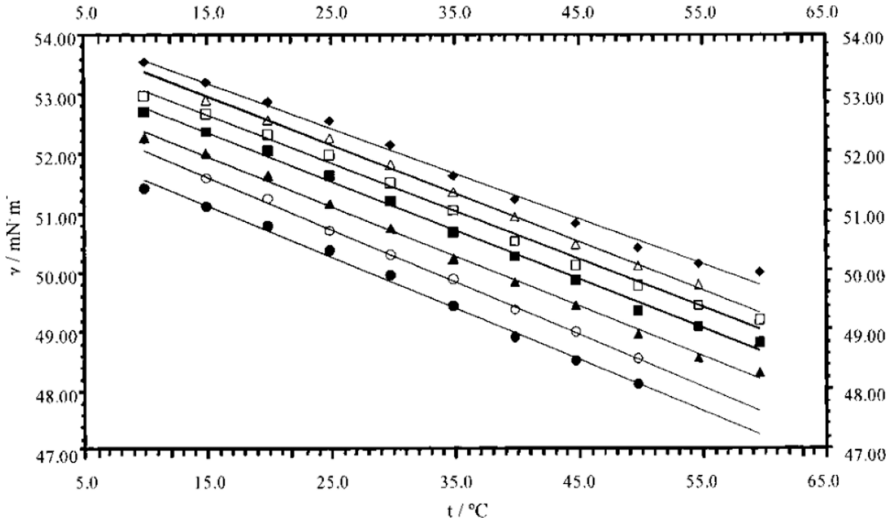

Figure 12. Interfacial tension values as a function of temperature for several *n*-alkanes: from the bottom to the top are hexane, heptane, octane, nonane, decane, undecane, and dodecane. Reprinted with permission from ref 70. Copyright 2001 American Chemical Society.

https://doi.org/10.1021/acsomega.3c00774
ACS Omega 2023, 8, 15479−15487

Finally, the desorption energy (ΔF) can be expressed as

$$\Delta F = \gamma_{o-w} \cdot (a^{u}_{o-w} - a'_{o-w} + a'_{o-c} \cdot \cos\theta) \quad (8)$$

The calculation of eq 8 shows that $\Delta F/\gamma_{o-w}$ fluctuates within the range of 17−22 nm^2. Considering the statistical error, $\Delta F/\gamma_{o-w}$ can be regarded as a constant. According to Zisman's theory,[69] γ_{o-w} can be a linear function of cos θ. This empirical correlation shows that the desorption energy (ΔF) can be approximated by a linear correlation of cos θ, as shown below

$$\Delta F \approx c_1 \cdot \cos\theta + c_2 \quad (9)$$

The MD simulation results in Section 2.5 show that the contact angle of diesel oil increases with temperature. Therefore, the desorption energy decreases with the increase of temperature. This indicates that the energy required for oil droplet desorption decreases with the increase of temperature. As a result, the oil droplets are difficult to adhere to and easier to desorb at high temperatures. The adsorption of the collector is stronger at low temperatures. Therefore, the flotation effect is better at low temperatures and worsened by high temperatures.

It is equally feasible to use the interface tension to directly explain this point without using Zisman theory. According to Zeppieri's data,[70] as shown in Figure 12, the interfacial tension of oil and water decreases with increasing temperature, and the pattern is very obvious and consistent for various oils. This can support the above conclusion.

According to the SEM and LP-N2A results, the pores and fractures of the coal sample are well developed. The interfacial tension between oil and water decreases with the increase of temperature, the oil droplet dispersity becomes better and the droplet size becomes smaller. According to the MSD results, the diffusion ability of oil droplets increases with the increase of temperature. At the same time, the viscosity of oil droplets decreases, and the fluidity increases.[33] These increase the volume of oil droplets that penetrate into the pores, resulting in the reduction of oil droplet spreading volume. This leads to the poor spreadability of oil droplets on the coal surface, which reduces the ability of oil droplets to cover oxygen-containing sites. The hydrophobicity of the coal surface is further reduced, thus worsening flotation.

Moreover, during the flotation process, we observed that the average volume of bubbles gradually increases as temperature rises, which renders the flotation foam unstable and worsens the flotation. The schematic diagram of the temperature effect mechanism is shown in Figure 13.

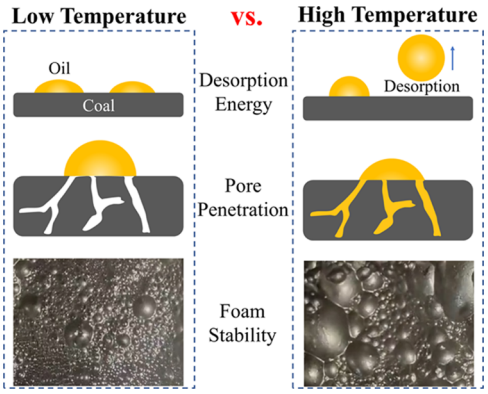

Figure 13. Schematic diagram of the temperature effect mechanism.

5. CONCLUSIONS

- The flotation rate slows down with the increase of temperature. The final combustible recovery gradually decreases as temperature rises. Low temperature is conducive to the flotation of LRC. Compared with 60 °C, the combustible recovery in flotation at 5 °C increases by 18.13%.
- The desorption energy for oil droplets decreases as the temperature rises. As a result, the oil droplets are difficult to adhere to and easier to desorb at high temperatures. The adsorption of the collector is stronger at low temperatures. Therefore, the flotation effect is better at low temperatures and worsened by high temperatures.
- The SEM and LP-N_2A results show that the pores and fractures of the coal sample are well developed. The interfacial tension between oil and water decreases with the increase of temperature, and the oil droplet dispersity becomes better. At the same time, the viscosity of oil droplets decreases, while the diffusion ability increases. These make the volume of oil droplets penetrating into the pores larger, resulting in poor spreading of oil droplets on the surface of coal.
- The average volume of bubbles gradually increases as the temperature rises, which would cause the flotation foam to become unstable and worsen the flotation.

AUTHOR INFORMATION

Corresponding Authors

Xicheng Bao − *Chinese National Engineering Research Center of Coal Preparation and Purification, Xuzhou, Jiangsu 221116, China; School of Chemical Engineering and Technology, China University of Mining and Technology, Xuzhou, Jiangsu 221116, China;* orcid.org/0000-0001-9421-0946; Email: baoxc246@gmail.com

Mengdi Xu − *Chinese National Engineering Research Center of Coal Preparation and Purification, Xuzhou, Jiangsu 221116, China*; Email: cumtxmd@outlook.com

Authors

Junling Liu − *Henan Energy Group Co., Ltd., Zhengzhou, Henan 450046, China*

Shasha Wang − *Chinese National Engineering Research Center of Coal Preparation and Purification, Xuzhou, Jiangsu 221116, China; School of Chemical Engineering and Technology, China University of Mining and Technology, Xuzhou, Jiangsu 221116, China*

Dongqin Chen − *Chinese National Engineering Research Center of Coal Preparation and Purification, Xuzhou, Jiangsu 221116, China; School of Chemical Engineering and Technology, China University of Mining and Technology, Xuzhou, Jiangsu 221116, China*

Wenjin Xu − *Chinese National Engineering Research Center of Coal Preparation and Purification, Xuzhou, Jiangsu 221116, China; School of Chemical Engineering and Technology, China University of Mining and Technology, Xuzhou, Jiangsu 221116, China*

Deke Zhang − *Chinese National Engineering Research Center of Coal Preparation and Purification, Xuzhou, Jiangsu 221116, China; School of Chemical Engineering and*

https://doi.org/10.1021/acsomega.3c00774
ACS Omega 2023, 8, 15479−15487

Technology, China University of Mining and Technology, Xuzhou, Jiangsu 221116, China

Jihui Li − *School of Chemical and Environmental Engineering, China University of Mining and Technology (Beijing), Beijing 100083, China;* orcid.org/0000-0002-4748-0692

Yaowen Xing − *Chinese National Engineering Research Center of Coal Preparation and Purification, Xuzhou, Jiangsu 221116, China*

Complete contact information is available at: https://pubs.acs.org/10.1021/acsomega.3c00774

Author Contributions

Conceptualization, J.L., X.B., and M.X.; methodology, J.L., J.L., and X.B.; validation, S.W. and D.C.; formal analysis, X.B. and M.X.; investigation, S.W.; resources, J.L.; data curation, D.Z. and W.X.; writing—original draft preparation, J.L. and X.B.; writing—review and editing, M.X. and Y.X.; funding acquisition, M.X. All authors have read and agreed to the published version of the manuscript.

Notes

The authors declare no competing financial interest.

■ ACKNOWLEDGMENTS

This research was funded by the Jiangsu Natural Science Fund-Youth Fund (BK20210500) and the National Nature Science Foundation of China (52104277). The authors would like to thank Wenxiang Wang from Shiyanjia Lab (www.shiyanjia.com) for the LP-N_2A measurements.

■ REFERENCES

(1) Shen, L.; Gong, J.; Liu, Y. Production of Ultra-Clean Coal by the Combined Method of Grinding and Collector Gasification Flotation. *Processes* **2022**, *10*, 2736.

(2) Zhang, R.; Xing, Y.; Xia, Y.; Guo, F.; Ding, S.; Tan, J.; Che, T.; Meng, F.; Gui, X. Synergistic Adsorption Mechanism of Anionic and Cationic Surfactant Mixtures on Low-Rank Coal Flotation. *ACS Omega* **2020**, *5*, 20630−20637.

(3) Lin, Q.; Mei, Y.; Huang, W.; Zhang, B.; Liu, K. Understanding the Role of Polyvinylpyrrolidone on Ultrafine Low-Rank Coal Flotation. *ACS Omega* **2022**, *7*, 10196−10204.

(4) Yang, A.; Liao, Y.; An, M.; Cao, Y.; Yang, Z.; Ren, H.; Su, H.; Zou, Q.; Chen, L. Effect of Ultrasonic Pretreatment on Flocculation Filtration of Low-Rank Coal Slurry. *Molecules* **2022**, *27*, 6460.

(5) Lu, F.; Liu, L.; Min, F.; Chen, J.; Zhang, M. Density Functional Theory Analysis of the Adsorption Interactions of Carbon Impurities in Coal-associated Kaolinite. *Processes* **2019**, *7*, 782.

(6) Duan, P.; Han, S.; Wang, W.; Tang, Y. Distribution and Migration of Trace Elements during Flotation in Ge-Rich Low-Rank Coal from Wulantuga Coal Mine, Inner Mongolia, China. *ACS Omega* **2022**, *7*, 2023−2030.

(7) Xu, C.; Wang, H.; Wang, D.; Zhu, X.; Zhu, Y.; Bai, X.; Yang, Q. Improvement of Foaming Ability of Surfactant Solutions by Water-Soluble Polymers: Experiment and Molecular Dynamics Simulation. *Polymers* **2020**, *12*, 571.

(8) Bao, X.; Xing, Y.; Liu, Q.; Liu, J.; Dai, S.; Gui, X.; Li, J.; Yang, Z. Investigation on mechanism of the oleic acid/methyl oleate/diesel ternary compound collector in low-rank coal flotation. *Fuel* **2022**, *320*, 123894.

(9) Ma, M.; Wang, W.; Zhang, K. Occurrence Characteristics of Fine-Grained Pyrite in Coal and Its Scaling Effect on Flotation Desulfurization. *ACS Omega* **2022**, *7*, 42467−42481.

(10) Bu, X.; Wang, X.; Zhou, S.; Li, B.; Zhan, H.; Xie, G. Discrimination of Six Flotation Kinetic Models Used in the Conventional Flotation and Carrier Flotation of -74 μm Coal Fines. *ACS Omega* **2020**, *5*, 13813−13821.

(11) Kong, Y.; Li, F.; Jia, Q.; Li, G. Application of Magnetization Treatment in Flotation. *J. Phys. Conf.* **2021**, *1748*, 062005.

(12) Wang, S.; Tao, X. Comparison of the adhesion kinetics between air or oily bubble and long flame coal surface in flotation. *Fuel* **2021**, *291*, 120139.

(13) Hu, H.; Li, M.; Li, L.; Tao, X. Improving bubble-particle attachment during the flotation of low rank coal by surface modification. *Int. J. Min. Sci. Technol.* **2020**, *30*, 217−223.

(14) Xing, Y.; Xu, M.; Gui, X.; Cao, Y.; Babel, B.; Rudolph, M.; Weber, S.; Kappl, M.; Butt, H.-J. The application of atomic force microscopy in mineral flotation. *Adv. Colloid Interface Sci.* **2018**, *256*, 373−392.

(15) Xing, Y.; Xu, M.; Gui, X.; Cao, Y.; Rudolph, M.; Butt, H.-J.; Kappl, M. The role of surface forces in mineral flotation. *Curr. Opin. Colloid Interface Sci.* **2019**, *44*, 143−152.

(16) Tian, Q.; Wang, H.; Pan, Y. Associations of Gangue Minerals in Coal Flotation Tailing and Their Transportation Behaviors in the Flotation Process. *ACS Omega* **2022**, *7*, 27542−27549.

(17) Zhang, L.; Guo, J.; Xie, Z.; Li, B.; Liu, S. Micro-mechanism of improving low-rank coal flotation by using carboxylic acid collector: A DFT calculation and MD simulation study. *Colloids Surf., A* **2021**, *622*, 126696.

(18) Li, W.; Wang, H.; Li, X.; Liang, Y.; Wang, Y.; Zhang, H. Effect of mixed cationic/anionic surfactants on the low-rank coal wettability by an experimental and molecular dynamics simulation. *Fuel* **2021**, *289*, 119886.

(19) Zhu, C.; Xing, Y.; Xia, Y.; Wang, Y.; Li, G.; Gui, X. Flotation intensification of low-rank coal using a new compound collector. *Powder Technol.* **2020**, *370*, 197−205.

(20) Niu, C.; Xia, W.; Li, Y.; Bu, X.; Wang, Y.; Xie, G. Insight into the low-rank coal flotation using amino acid surfactant as a promoter. *Fuel* **2022**, *307*, 121810.

(21) Xue, Z.; Dong, L.; Li, H.; Fan, M.; Ren, Z.; Liu, A.; Fan, P.; Bao, W. Study on the mechanism of flotation of coal gasification fine slag reinforced with naphthenic acids. *Fuel* **2022**, *324*, 124557.

(22) Liao, Y.; Yang, Z.; An, M.; Ma, L.; Yang, A.; Cao, Y.; Chen, L.; Ren, H. Alkanes-esters mixed collector enhanced low rank coal flotation: Interfacial interaction between oil drop and coal particle. *Fuel* **2022**, *321*, 124045.

(23) Zhang, Q.; Niu, C.; Bu, X.; Bilal, M.; Ni, C.; Peng, Y. Enhancement of Flotation Performance of Oxidized Coal by the Mixture of Laurylamine Dipropylene Diamine and Kerosene. *Minerals* **2021**, *11*, 1271.

(24) Liao, Y.; Song, X.; An, M.; Yang, Z.; Hao, X.; Ren, H. Effect of Dodecane-Oleic Acid Collector Mixture on the Evolution of Wetting Film between Air Bubble and Low-Rank Coal. *Minerals* **2021**, *11*, 58.

(25) An, M.; Liao, Y.; Cao, Y.; Hao, X.; Ma, L. Improving Low Rank Coal Flotation Using a Mixture of Oleic Acid and Dodecane as Collector: A New Perspective on Synergetic Effect. *Processes* **2021**, *9*, 404.

(26) Kang, H.; Zhang, H. Enhanced Flotation Separation of Low-Rank Coal with a Mixed Collector: Experimental and Molecular Dynamics Simulation Study. *ACS Omega* **2022**, *7*, 34239−34248.

(27) Huang, G.; Xu, J.; Geng, P.; Li, J. Carrier Flotation of Low-Rank Coal with Polystyrene. *Minerals* **2020**, *10*, 452.

(28) Yao, N.; Liu, J.; Sun, X.; Liu, Y.; Chen, S.; Wang, G. A Rational Interpretation of the Role of Turbulence in Particle-Bubble Interactions. *Minerals* **2021**, *11*, 1006.

(29) Zhou, W.; Wang, S.; Wang, L.; Cai, C.; Li, J.; Liu, L.; Zhu, J.; Min, F. Study on Dispersion and Mixing Mechanism of Coal Slime Particles in Jet Mixing Flow Field. *Minerals* **2023**, *13*, 13.

(30) Wang, H.; Yang, W.; Li, D.; Zhang, C.; Yan, X.; Wang, L.; Zhang, H. Enhancement of coal flotation using impact flow conditioning pulp. *J. Clean. Prod.* **2020**, *267*, 122124.

(31) Han, Y.; Wang, X.; Zhu, J.; Wang, P. Gas Dispersion Characteristics in a Novel Jet-Stirring Coupling Flotation Device. *ACS Omega* **2022**, *7*, 9061−9070.

(32) Li, D.; Zhang, C.; Li, X.; Yang, L.; Yan, X.; Wang, L.; Liu, Q.; Zhang, H. Experimental study on the preconditioning of fine coal

particles surface modification using a new type flow mixer. *Fuel* **2020**, *268*, 117361.
(33) Hacifazlioglu, H. Effect of Temperature on Coal Flotation with Waste Vegetable Oil as Collector. *Int. J. Coal Prep. Util.* **2018**, *38*, 163−169.
(34) Xia, Y.; Zhang, R.; Cao, Y.; Xing, Y.; Gui, X. Role of molecular simulation in understanding the mechanism of low-rank coal flotation: A review. *Fuel* **2020**, *262*, 116535.
(35) Xia, Y.; Rong, G.; Xing, Y.; Gui, X. Synergistic adsorption of polar and nonpolar reagents on oxygen-containing graphite surfaces: Implications for low-rank coal flotation. *J. Colloid Interface Sci.* **2019**, *557*, 276−281.
(36) Zhang, L.; Sun, X.; Li, B.; Xie, Z.; Guo, J.; Liu, S. Experimental and molecular dynamics simulation study on the enhancement of low rank coal flotation by mixed collector. *Fuel* **2020**, *266*, 117046.
(37) Liu, Z.; Ren, H.; Yang, Z.; Liao, Y.; Cao, Y. Effect of mixed collector addition sequence on the adsorption behavior of low-rank coal surface: Experimental and molecular dynamics simulation study. *Powder Technol.* **2022**, *397*, 117119.
(38) Xia, Y.; Xing, Y.; Li, M.; Liu, M.; Tan, J.; Cao, Y.; Gui, X. Studying interactions between undecane and graphite surfaces by chemical force microscopy and molecular dynamics simulations. *Fuel* **2020**, *269*, 117367.
(39) Zhong, J.; Wang, X.; Du, J.; Wang, L.; Yan, Y.; Zhang, J. Combined Molecular Dynamics and Quantum Mechanics Study of Oil Droplet Adsorption on Different Self-Assembly Monolayers in Aqueous Solution. *J. Phys. Chem. C* **2013**, *117*, 12510−12519.
(40) Vassetti, D.; Pagliai, M.; Procacci, P. Assessment of GAFF2 and OPLS-AA General Force Fields in Combination with the Water Models TIP3P, SPCE, and OPC3 for the Solvation Free Energy of Druglike Organic Molecules. *J. Chem. Theory Comput.* **2019**, *15*, 1983−1995.
(41) Wang, J.; Wolf, R. M.; Caldwell, J. W.; Kollman, P. A.; Case, D. A. Development and testing of a general amber force field. *J. Comput. Chem.* **2004**, *25*, 1157−1174.
(42) Abraham, M. J.; Murtola, T.; Schulz, R.; Páll, S.; Smith, J. C.; Hess, B.; Lindahl, E. GROMACS: High performance molecular simulations through multi-level parallelism from laptops to supercomputers. *SoftwareX* **2015**, *1−2*, 19−25.
(43) Neese, F.; Wennmohs, F.; Becker, U.; Riplinger, C. The ORCA quantum chemistry program package. *J. Chem. Phys.* **2020**, *152*, 224108.
(44) Schauperl, M.; Nerenberg, P. S.; Jang, H.; Wang, L.-P.; Bayly, C. I.; Mobley, D. L.; Gilson, M. K. Non-bonded force field model with advanced restrained electrostatic potential charges (RESP2). *Commun. Chem.* **2020**, *3*, 44.
(45) Lu, T.; Chen, F. Multiwfn: a multifunctional wavefunction analyzer. *J. Comput. Chem.* **2012**, *33*, 580−592.
(46) Pandit, S.; Maroli, N.; Naskar, S.; Khatri, B.; Maiti, P. K.; De, M. Graphene oxide as a dual template for induced helicity of peptides. *Nanoscale* **2022**, *14*, 7881−7890.
(47) Lu, T. Sobtop, Version 1.0(dev3). http://sobereva.com/soft/Sobtop (accessed 26 Mar, 2022).
(48) Zimmermann, K. ORAL: All purpose molecular mechanics simulator and energy minimizer. *J. Comput. Chem.* **1991**, *12*, 310−319.
(49) Bussi, G.; Donadio, D.; Parrinello, M. Canonical sampling through velocity rescaling. *J. Chem. Phys.* **2007**, *126*, 014101.
(50) Hess, B.; Bekker, H.; Berendsen, H. J. C.; Fraaije, J. G. E. M. LINCS: A linear constraint solver for molecular simulations. *J. Comput. Chem.* **1997**, *18*, 1463−1472.
(51) Essmann, U.; Perera, L.; Berkowitz, M. L.; Darden, T.; Lee, H.; Pedersen, L. G. A smooth particle mesh Ewald method. *J. Chem. Phys.* **1995**, *103*, 8577−8593.
(52) Humphrey, W.; Dalke, A.; Schulten, K. VMD: Visual molecular dynamics. *J. Mol. Graph.* **1996**, *14*, 33−38.
(53) Pietrzak, R.; Wachowska, H. Low temperature oxidation of coals of different rank and different sulphur content. *Fuel* **2003**, *82*, 705−713.
(54) Pietrzak, R.; Wachowska, H. Thermal analysis of oxidised coals. *Thermochim. Acta* **2004**, *419*, 247−251.
(55) Orrego-Ruiz, J. A.; Cabanzo, R.; Mejía-Ospino, E. Study of Colombian coals using photoacoustic Fourier transform infrared spectroscopy. *Int. J. Coal Geol.* **2011**, *85*, 307−310.
(56) Sokolovic, J. M.; Stanojlovic, R. D.; Markovic, Z. S. Activation of oxidized surface of anthracite waste coal by attrition. *Physicochem. Probl. Miner. Process.* **2012**, *48*, 5−18.
(57) Zhou, S.; Liu, D.; Cai, Y.; Yao, Y. Fractal characterization of pore−fracture in low-rank coals using a low-field NMR relaxation method. *Fuel* **2016**, *181*, 218−226.
(58) Li, T.; Wu, C.-F.; Wang, Z.-W. The dynamic change of pore structure for low-rank coal under refined upgrading pretreatment temperatures. *Pet. Sci.* **2021**, *18*, 430−443.
(59) Liu, D.; Qiu, F.; Liu, N.; Cai, Y.; Guo, Y.; Zhao, B.; Qiu, Y. Pore structure characterization and its significance for gas adsorption in coals: A comprehensive review. *Unconv. Resour.* **2022**, *2*, 139−157.
(60) Grzybek, T.; Pietrzak, R.; Wachowska, H. X-ray photoelectron spectroscopy study of oxidized coals with different sulphur content. *Fuel Process. Technol.* **2002**, *77−78*, 1−7.
(61) Chen, X.; Wang, X.; Fang, D. A review on C1s XPS-spectra for some kinds of carbon materials. *Fullerenes, Nanotubes, Carbon Nanostruct.* **2020**, *28*, 1048−1058.
(62) Xing, Y.; Zhang, Y.; Liu, M.; Xu, M.; Guo, F.; Han, H.; Gao, Z.; Cao, Y.; Gui, X. Improving the floatability of coal with varying surface roughness through hypobaric treatment. *Powder Technol.* **2019**, *345*, 643−648.
(63) Xing, Y.; Gui, X.; Cao, Y.; Wang, Y.; Xu, M.; Wang, D.; Li, C. Effect of compound collector and blending frother on froth stability and flotation performance of oxidized coal. *Powder Technol.* **2017**, *305*, 166−173.
(64) Cai, Y.; Du, M.; Wang, S.; Liu, L. Flotation characteristics of oxidized coal slimes within low-rank metamorphic. *Powder Technol.* **2018**, *340*, 34−38.
(65) Zhang, Z.; Stephens, A.; Wang, J. Temperature Effect on Interactions of Oil Droplet with Water-wetted Shale Kerogen at Reservoir Temperatures: Linear Relationships between Temperature, Free Energy, and Contact Angle. **2020**, arXiv:2007.09741.
(66) Gayle, J. B.; Smelley, A. G. *Effects of Temperature Variations on Contact Angles for Coal and Related Substances*; U.S. Department of the Interior, Bureau of Mines, 1960.
(67) Hung, S.-W.; Hsiao, P.-Y.; Chen, C.-P.; Chieng, C.-C. Wettability of Graphene-Coated Surface: Free Energy Investigations Using Molecular Dynamics Simulation. *J. Phys. Chem. C* **2015**, *119*, 8103−8111.
(68) Das, S. K.; Binder, K. Does Young's equation hold on the nanoscale? A Monte Carlo test for the binary Lennard-Jones fluid. *Europhys. Lett.* **2010**, *92*, 26006.
(69) Fox, H.; Zisman, W. The spreading of liquids on low-energy surfaces. III. Hydrocarbon surfaces. *J. Colloid Sci.* **1952**, *7*, 428−442.
(70) Zeppieri, S.; Rodríguez, J.; López de Ramos, A. L. Interfacial Tension of Alkane + Water Systems. *J. Chem. Eng. Data* **2001**, *46*, 1086−1088.

https://doi.org/10.1021/acsomega.3c00774
ACS Omega 2023, 8, 15479−15487